A Small Array of Boresight to Endfire Radiation Reconfigurable Antennas[1]

G. H. Huff, J. Feng, and J. T. Bernhard

Electromagnetics Laboratory
Department of Electrical and Computer Engineering
University of Illinois at Urbana-Champaign
Urbana, IL 61801

Abstract

This work describes the development of a 2x2 array of pattern reconfigurable antennas, capable of switching between boresight and endfire radiation patterns over a common impedance bandwidth. The reconfigurable element for the array is a single turn square spiral microstrip antenna on an electrically thin substrate, and is capable of reconfiguring its radiation pattern from boresight to endfire using two surface-mounted switching elements. An outline of the theory developed for standing wave devices to generate reconfigurable pattern behavior is also included. Application of the antenna array to geosynchronous satellites is also provided.

1. Introduction

Reconfigurable behavior of an antenna can manifest itself in a variety of different and useful forms. The desired properties of such an antenna may range from manipulation of the frequency response all the way to changing the radiation characteristics (such as pattern or polarization). Coinciding with the development and practicality of the reconfigurable antenna, reliable switching technologies continue to advance, providing endless possibilities for their application to future integrated antenna designs. As a result, systems that these antennas support are

[1] This work is supported by NASA under research agreement #NAG3-2555 and the National Science Foundation under grant #ECS 99-83460.

likely to advance as well, or simply become smaller, lighter and considerably less expensive due to the increased functionality that comes with reconfigurability.

For the array of reconfigurable radiation elements discussed in this work, the pattern is reconfigured from boresight to endfire over a common impedance bandwidth. To develop a pattern reconfigurable array, the single element is discussed first and a model is presented that outlines the reconfigured radiation characteristics and geometry of the antenna. Measurements of the single element's radiation patterns and impedance are given next. Following this, the settings needed for the array to recover the reconfigured radiation characteristics of the single element are determined using pattern multiplication of the array factor and the individual element patterns. After the proper array settings have been determined, the 2x2 array is fabricated and measurements of the radiation patterns and the VSWR of the individual elements are presented. The final two sections provide a brief discussion on the application of the small array of reconfigurable elements to geosynchronous satellites and mobile communications and a summary of the work and possibilities for future work.

2. Element Characteristics

With an increasing amount of reconfigurable antennas under development, only a limited amount of research has been presented to characterize their operation. As a result, many of these devices become a challenge to formalize into a specific design process, making them somewhat enigmatic to scale and tune for individual applications. To develop a better understanding of the electromagnetics driving the pattern reconfigurable antenna discussed in this work, and gain insight into the fundamental operation of the device, an effective model of a standing wave reconfigurable antenna is presented.

2.1 Model Outline

To develop an effective model for the radiation reconfigurable antenna, the reconfigured pattern characteristics of the antenna become the defining parameter. For the antenna in this work, the desired radiation pattern is to be switched between boresight and endfire directions (relative to the antenna), and is to occur over a common impedance bandwidth. To capture this functionality, the model begins with a few observations about the geometry (shown in Figure 1) and operation of the antenna; a) the antenna is a standing wave device, b) the standing surface current distribution occurs only along the length of the line, and c) the standing current density that facilitates radiation can be replaced by a set of equivalent dipoles. The resulting reconfigured pattern behavior may be predicted

via pattern superposition of the equivalent dipole patterns. Using these guidelines, a model can be developed to enable this class of devices to reconfigure themselves for almost any type of operation.

The analysis begins with an examination of the standing current density for a given geometry. Using this distribution, the modal structure of the current density is replaced by an appropriate series of dipoles positioned appropriately at the location of the anti-nodes. Given a geometry that supports this modal current distribution, the linear separation of these equivalent dipoles is a half wavelength. Utilizing the geometry as a degree of freedom, these dipole moments are then given a specific orientation and phase provided by the sign of the anti-node. For a well designed geometry and placement of anti-nodes, array theory can simplify the characterization of the radiation pattern. Then, assuming the means are available through alteration of geometric character, the reconfigured pattern is achieved by modifying the current distribution, resulting in a phase shift between the equivalent dipoles that can then facilitate changes in radiation characteristics.

2.2 Antenna Geometry

The base geometry for the antenna is a single turn square microstrip spiral antenna [1, 2], which supports a standing wave on an electrically thin substrate. and is similar to the antenna in [3, 4, 5]. The antenna geometry along with the accompanying switching element positions can be seen in Figure 1 with the associated parameters in Table 1. The linear dimension of the antenna is 81 mm, approximately two wavelengths at the desired frequency and is fabricated on Duroid 5880 substrate ($\varepsilon_r = 2.2$) with height h = 3.175 mm (~0.072λ @ 6.8 GHz). A vertical SMA probe feed of diameter 1.23 mm is used to feed the antenna, which is shorted to ground at the opposing linear dimension using a via of diameter 1.23 mm. To alter the current distribution on the structure and reconfigure the radiation pattern, two surface mountable in-line switching elements of dimension 1.0mm x 1.0mm (currently hard wired for proof of concept) are incorporated into the design. For impedance tuning, the location of these switching elements can be carefully adjusted to achieve the correct impedance. To fully describe the reconfigured radiation, the antenna is examined for the two configurations used to reconfigure the radiation pattern from boresight to endfire over a shared impedance bandwidth. The first configuration discussed is that for the endfire radiation characteristics, followed by the boresight radiation configuration.

2.2.1 Endfire Configuration

In the endfire configuration, the switch at c' is closed and the switch at e' is open, yielding a total linear length of 81 mm. At this length, the antenna is approximately two wavelengths long at the design frequency of 6.8 GHz, and represents the second full standing wave mode of the antenna. Examination of the current distribution at this frequency places the resulting equivalent dipoles approximately at the corners of the structure (with a slight offset generated by the probe feed through the substrate). Since the standing current density lies on the corners, the resulting dipoles can be split into the two principle polarizations in the E-plane (xz) and H-plane (yz). With these current distributions representing the different polarizations, the equivalent sets of dipoles can be viewed as an array of dipoles that are spaced one half wavelength apart with a progressive phase difference of 180 degrees. The resulting radiation pattern can then be easily approximated as having endfire radiation characteristics using pattern multiplication.

2.2.2 Boresight Configuration

In the broadside configuration, the switch at c' is open and the switch at e' is closed, yielding a total linear length of 41 mm connected to the SMA probe feed, and 42.25 mm connected to the via to ground. In this configuration the antenna appears as two coupled single wavelength resonators, where the overlap between the two sections resembles a variation on a quarter wave coupled line filter. The SMA probe fed portion of the antenna acts as the driven portion of the coupled structure, with the grounded parasitic arm coupling the energy through the overlapping section, which is approximately one quarter of a guided wavelength. Since the coupling across the separation 's' represents a differential mode transfer of energy, the phase of the resulting currents on the parasitic arm are reversed and are 180 degrees out of phase from the probe fed section. By changing the phase of these currents on the parasitic arm, the resulting dipole arrangement is reversed, and hence the pattern is reconfigured. The analysis of the radiation characteristics is slightly different from the endfire configuration due to the standing current density being slightly shifted away from the corners on the parasitic section, but can be simplified to gain understanding of the radiation characteristics. With this slight shift off the corners and the increased magnitude of the currents on the parasitic section due to the coupling effects, a different distribution of magnitudes for the resulting set of dipoles occurs. Assuming that the current distribution is much greater on the parasitic arm, the currents on the driven section can be neglected, leaving only two orthogonal dipole orientations. This resulting dipole representation then yields an approximate boresight pattern.

2.3 Single Element Measurements

Measurements of the input impedance, VSWR, and radiation characteristics can be seen in Figures 3, 4, and 5 respectively (of the single element). Examining the plot of the VSWR for both configurations shows a shared impedance bandwidth of 96 MHz (1.39% BW), centered at 6.913 GHz. Examination of the radiation characteristics shows good agreement with the predicted pattern behavior from the dipole representation. In the boresight configuration, a tilt in the pattern is attributed to the relative magnitude difference in the dipole approximation (in which the contribution from the driven section was neglected), but the boresight characteristics are still maintained.

3. Array Configuration

For the array of reconfigurable antennas, several factors were examined to provide the necessary conditions needed by the two configurations in order to recover the functionality of the reconfigured antennas in an array setting. For this, the array factors for several different spacing and phasing scenarios were considered. Among these, two different array settings are considered along with the ground plane dimensions of the array.

3.1 Array Spacing

The array factors for each of the two array settings can be seen in Figure 6. To determine the relative performance tradeoffs of the two configurations, pattern multiplication between the single element pattern and the array factor has been used. The first array setting (Figure 6a) has a spacing that provides major lobes in the boresight and endfire directions, and uses the element pattern to dictate the peak and null directions. This spacing has several drawbacks however, including a full wavelength spacing (leading to a sparse array), and poor pattern control due to the onset of grating lobes from spacing and non-ideal pattern characteristics of the single element. To avoid these pitfalls, a better solution is found by spacing the elements one-half a wavelength apart (Figure 6b), and progressively phasing the elements in the endfire configuration 180° (Figure 6c). Doing so will result in an endfire pattern in the direction of progressive phasing, which will be addressed separately in both the E-plane and H-plane measurements. Although this array setting incorporates the additional complexity of phase shifters, both radiation configurations can be recovered. Consequently, the inter-element spacing in the array is quite small in the E-plane and H-plane, 3.8 mm (0.087λ) and 1.55 mm

(0.036λ) respectively, which will generate considerable effects on the performance of the array elements.

3.2 Ground Plane Dimensions

Along with the primary operating conditions (spacing, phasing, inter-element coupling, etc.), the ground plane dimensions are also examined and have shown significant effects on the performance of the array. Initial considerations of the ground plane dimensions arise from the desired performance of the array. For this particular antenna and array, a squinting of the endfire radiation away from the plane of the antenna has been seen in the single element when the ground plane dimension exceeds half a wavelength from all edges of the element, and is attributed to the far field beam forming restraints placed on it by the ground plane, similar to the squinted radiation pattern of a monopole over a finite ground plane. Therefore, effects from the asymmetrical placement of the elements on the larger ground plane of the array are also likely to influence the overall radiation characteristics of the array.

4. Experimental Results of the 2x2 Array

4.1 Common Impedance Bandwidth

Measurements of the VSWR for the endfire and boresight configurations can be seen in Figures 7 and 8 for the array. Earlier predictions of performance issues arising from inter-element coupling can be seen in the shifting and expansion of the VSWR bandwidths for the individual elements. Specifically, the upper and lower elements in the array show trends for each configuration depending on the row in which they reside. Since the dimension between rows (y-direction) is several times smaller than the column spacing (x-direction), the effect is much more pronounced in the rows of elements. This trend is especially evident in the boresight configuration where the quarter wave coupling section plays a key role in the operation of the individual elements. In total, the common impedance bandwidth is slightly broadened to 98.0 MHz (1.43% BW) with a shifted center frequency of 6.845 GHz.

4.2 Radiation Characteristics

Measurements of the radiation patterns for the endfire and boresight configurations can be seen in Figures 9 and 10 for the array. In the boresight configuration, the array performs well with minimal side lobes and an overall gain of 12.4 dBi. For all of the measured patterns, the maximum radiation occurs in

this configuration, and all endfire patterns are shown relative to this maximum. In the endfire configuration, the phasing in the E-plane and H-plane both generate well formed endfire radiation characteristics. The effect of ground plane dimensions can be seen in the radiation patterns for the endfire configuration for both the E-plane and H-plane phasing. For each of these patterns (Figure 10a and 10d), the maximum radiation occurs off of true endfire $\left(\theta = 90^\circ, \phi = 0^\circ, 180^\circ \left(E-plane\right) \text{ and } 90^\circ, 270^\circ \left(H-plane\right)\right)$, at approximately $\theta = 60^\circ$ with a gain of 9.52 dBi and 9.42 dBi for the E-plane and H-plane phasing respectively (also where the single element experiences a maximum endfire gain). For the total reconfigured pattern characteristics, the best operation is found in the phased E-plane setting where the resulting reconfigured pattern is linearly polarized in the cross-polarization and has a broad coverage.

5. Application

For the reconfigurable antenna presented, application to communication with geosynchronous satellites is considered as a possible application. Using the antenna in a small array setting, the coverage possible extends across the horizon and can be shifted towards the appropriate horizontal direction via the phasing in the x or y- directions. In doing so, communication through tunnels and during steep inclines or grades can be improved by reconfiguring the main beam towards the best possible reception which may not be directly overhead. Several drawbacks also arise from using an antenna with predominantly linear radiation characteristics because most down linked signals are broadcast in circular polarization. However, for linearly polarized signals the effects of multi-path should allow the antenna to operate effectively in most settings.

6. Conclusions

In this work, a 2x2 array of boresight to endfire pattern reconfigurable elements has been successfully demonstrated. In doing so, it has also been confirmed that the functionality of the individual reconfigurable elements can be recovered through judicious array planning, including spacing and phasing. Along with the array behavior of the individual elements, a model to describe the reconfigured radiation characteristics of the individual elements has also been developed and is in good agreement with the simulated and measured results. Future work for this antenna includes frequency and substrate scaling as well as integration with RF MEMS as well as other switching possibilities. Along with the physical parameters effecting the performance of the antenna, issues such as beam steering and grating lobes are also being considered.

7. Work Cited

[1] G. H. Huff, J. Feng, S. Zhang, J. T. Bernhard, "A Novel Radiation Pattern and Frequency Reconfigurable Single Turn Square Spiral Antenna," IEEE Microwave and Wireless Components Letters, vol.13, no. 2, pp. 57-60, Feb. 2003.

[2] G. H. Huff, J. Feng, J. T. Bernhard, "Theory and Measurement of a Radiation Reconfigurable Antenna," Submitted to IEEE Transactions on Antennas and Propagation.

[3] H. Nakano, S. Okuzawa, K. Ohishi, H. Mimaki, and J. Yamauchi, " A curl antenna," *IEEE Trans. Antennas Propagat.*, vol. 41, pp. 1570-1575, Nov. 1993.

[4] H. Nakano and H. Mimaki, " Axial ratio of a curl antenna," *IEE Proc.-Microw. Antennas Propag.*, vol. 144, pp. 488-490, Dec. 1997.

[5] C. Huang and K. Wong, "Stripline-fed printed square spiral slot antenna for circular polarization," *Electronic Letters*, vol. 34, pp. 2290-2292, Nov. 1998.

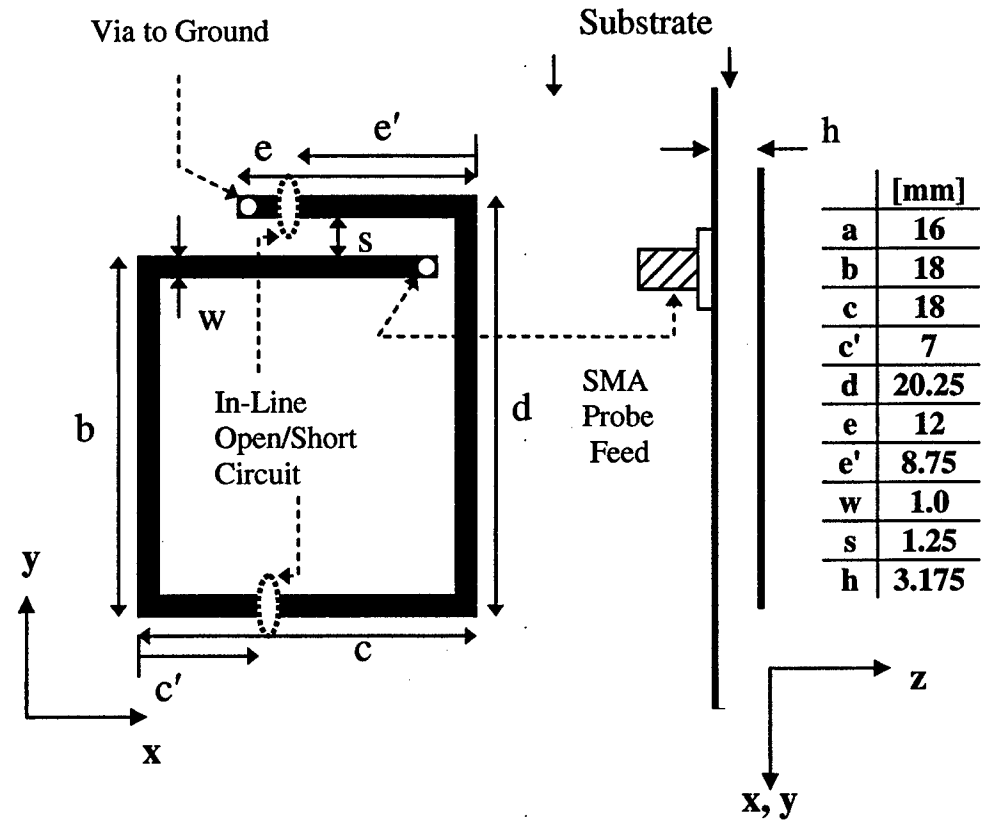

	[mm]
a	16
b	18
c	18
c'	7
d	20.25
e	12
e'	8.75
w	1.0
s	1.25
h	3.175

Figure 1. (Left) Antenna geometry and orientation for reconfigured pattern operation, (Right) list of given dimensions for the square spiral antenna. In the endfire configuration, the switch at e' is open and the switch at c' is closed, forming the square spiral geometry. For the boresight configuration the switch at c' is open and the switch at e' is closed, breaking the spiral and shorting the parasitic arm. In the orientation above, the E-plane is the xz-plane and the H-plane is the yz-plane.

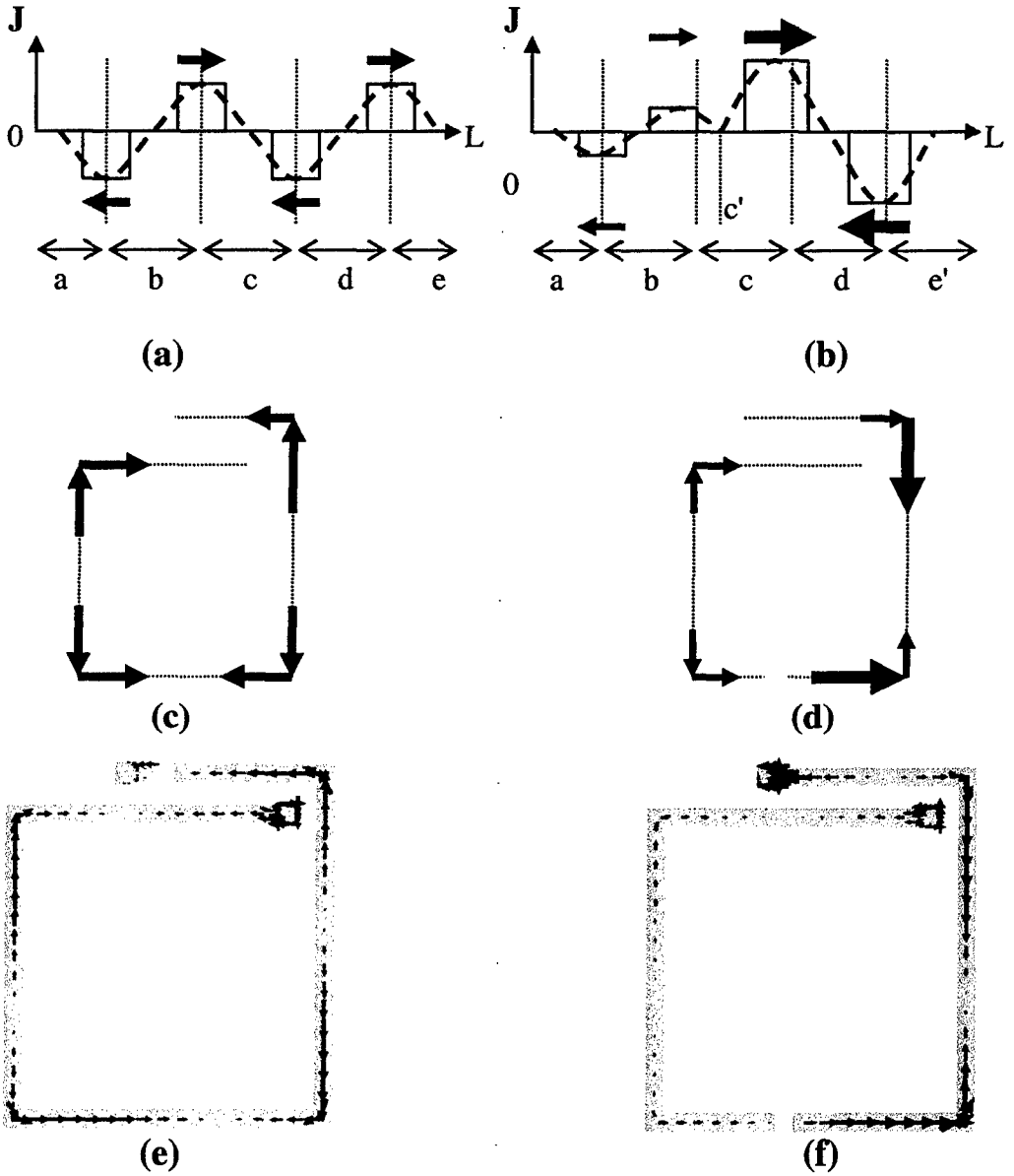

Figure 2. Graphical model for the prediction of radiation patterns via the mode structure of the current density **J** on spiral for the two configurations, endfire on left and boresight on right; (a) and (b) The approximate sinusoidal current distribution behavior of and equivalent set of dipoles, (c) and (d) Currents are mapped to the spiral geometry, resulting in the dipole array for use in the prediction of the radiation characteristics, (e) and (f) IE3D simulations of the surface current density on the two spiral geometries.

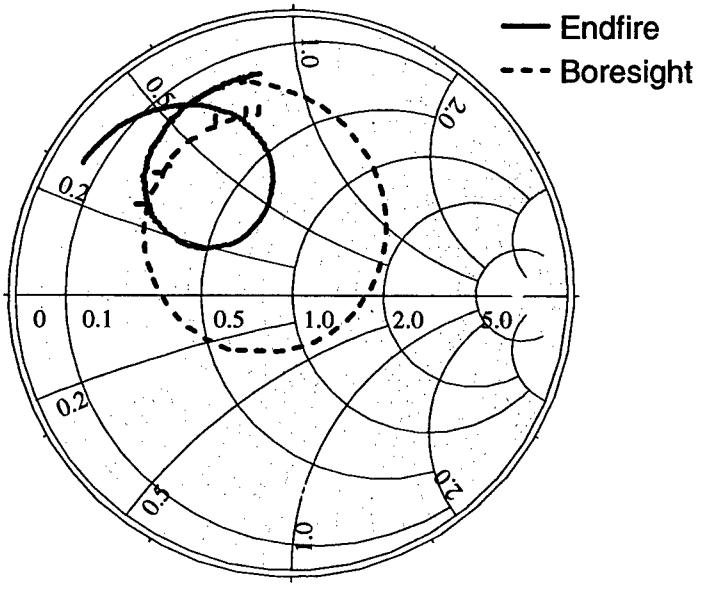

Figure 3. Measured input impedance of the endfire (solid) and boresight (dashed) configurations.

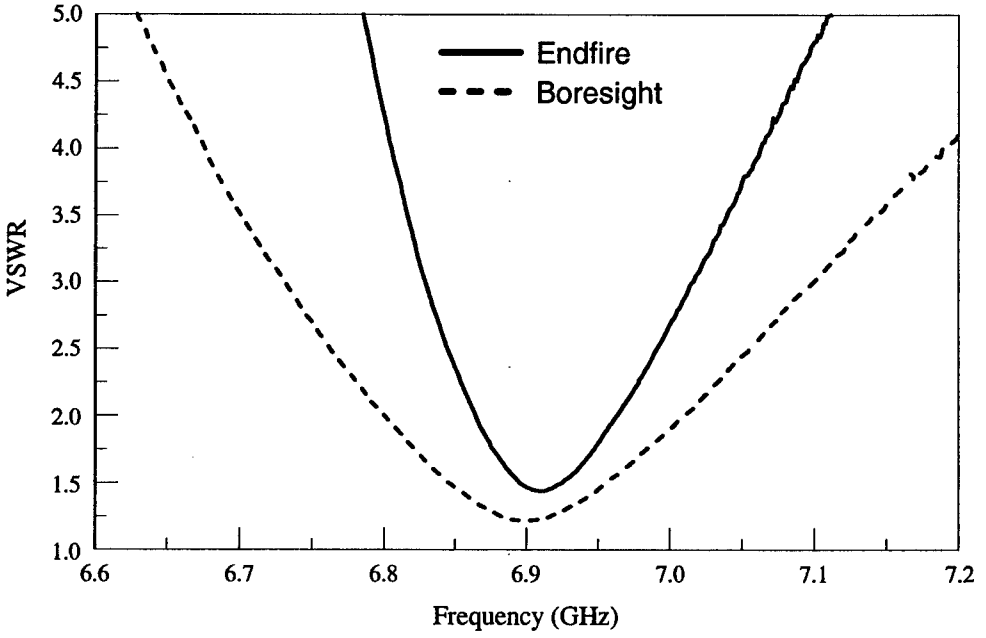

Figure 4. Measured VSWR of endfire (solid) and boresight (dashed) configurations with a common impedance bandwidth of 96 MHz (1.39 % BW) centered at 6.913 GHZ.

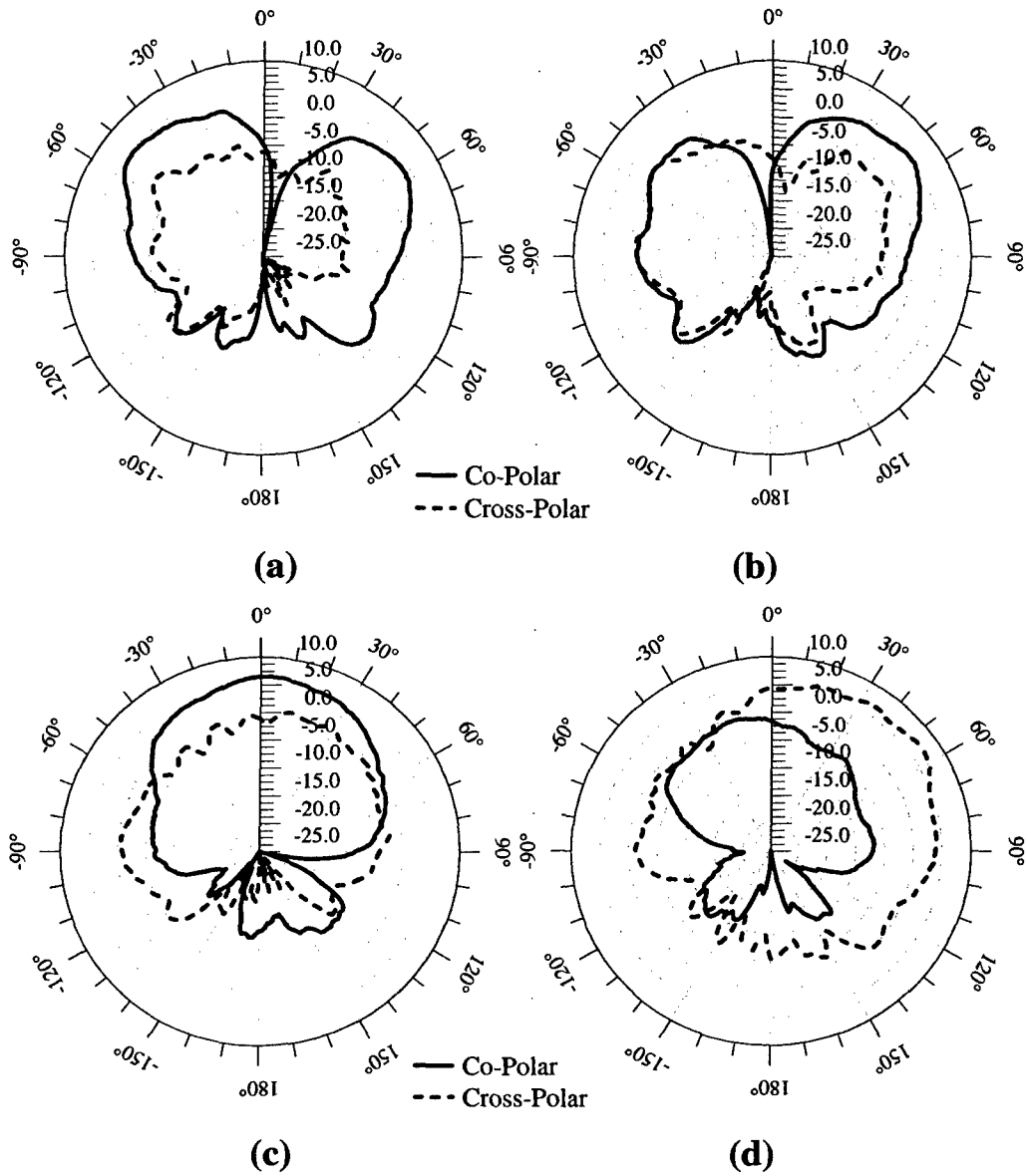

Figure 5. Measured single element radiation patterns for the (a) Endfire E-plane, (b) Endfire H-plane, (c) Boresight E-plane, and (d) Boresight H-plane.

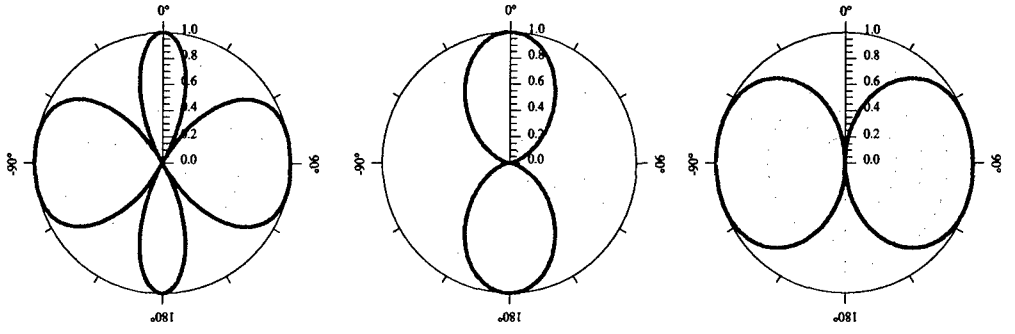

(a) **(b)** **(c)**

Figure 6. Two element array factors used to determine the operational characteristics of the antenna in an array setting; (a) configuration 1 uses a full wavelength spacing and is un-phased, (b) and (c) configuration 2 uses a half-wavelength spacing and is un-phased and progressively phased 180 degrees for the boresight and endfire configurations respectively.

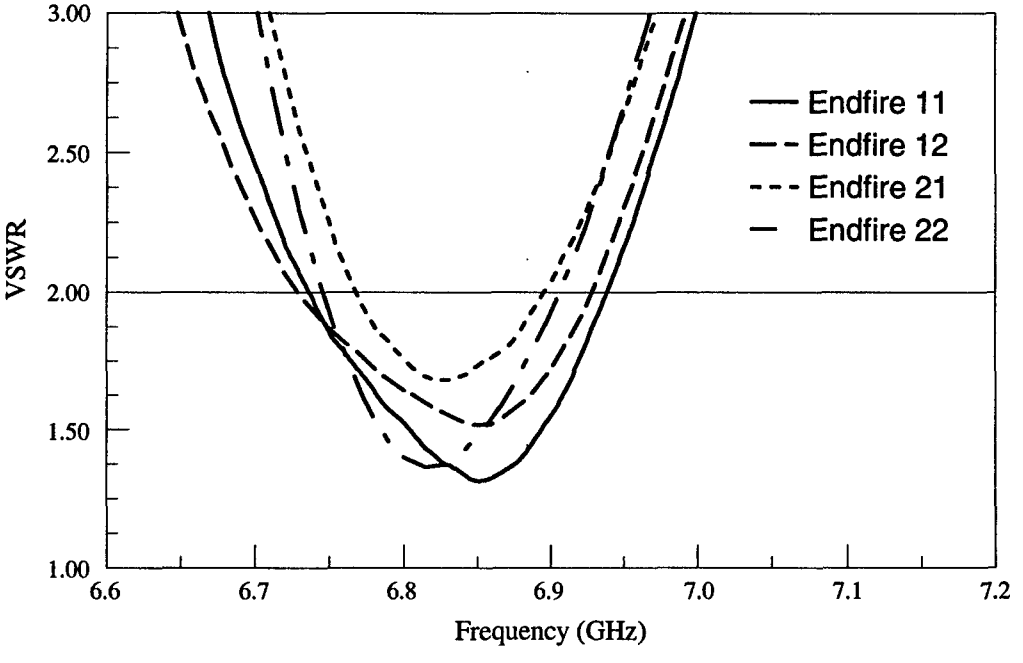

Figure 7. Measured VSWR of the array comprised of endfire configured elements. In the endfire configuration, the upper row of elements (11 and 12) experience a slight broadening of bandwidth, which is more pronounced in the lower row of elements (21 and 22). This is a result of the inter-element coupling.

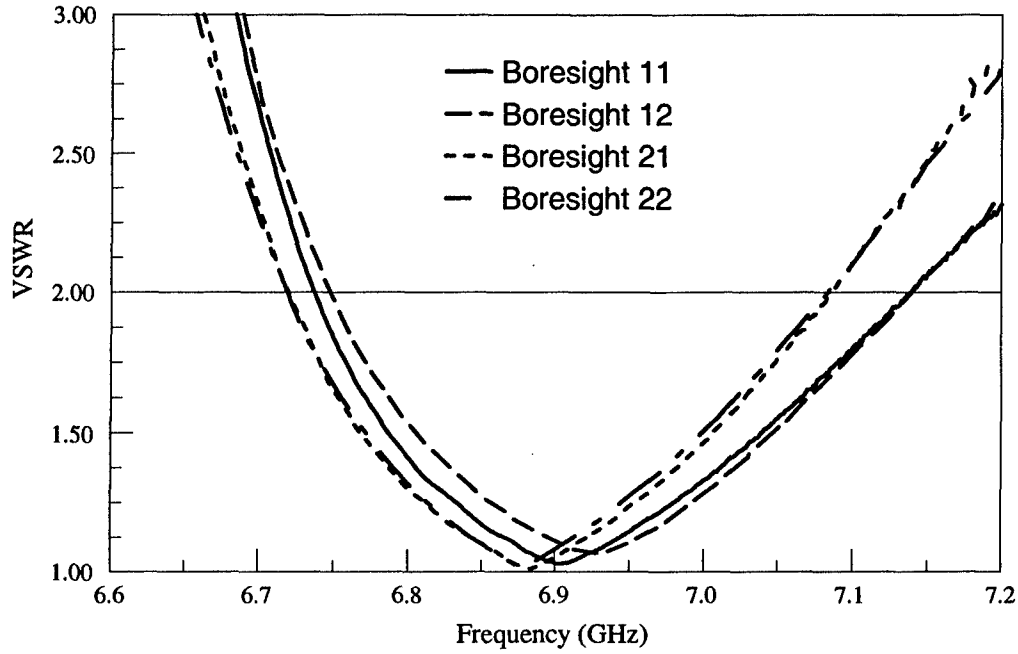

Figure 8. Measured VSWR of the array comprised of boresight configured elements. Note the trends in the upper row of elements (11 and 12) and lower the lower row of elements (21 and 22) due to the inter-element coupling.

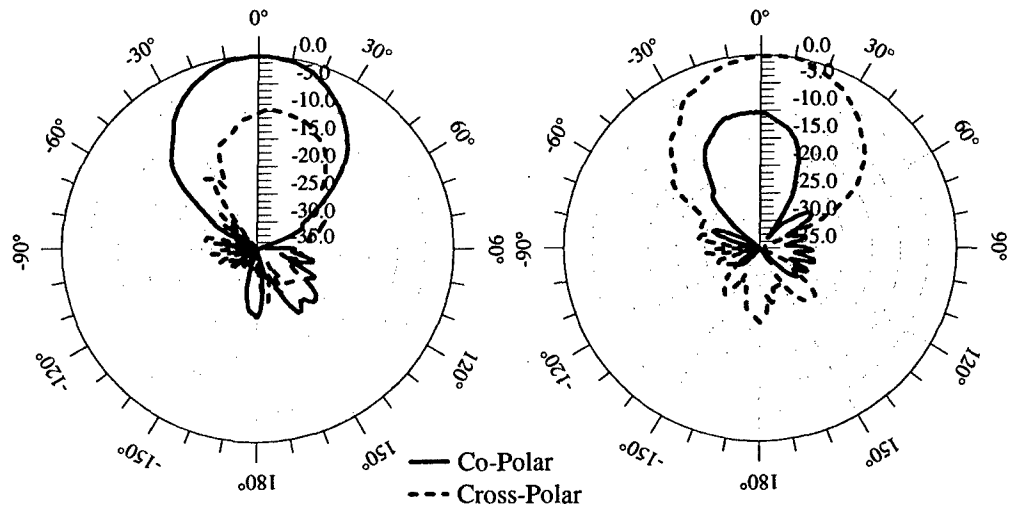

Figure 9. Measured (a) E-plane and (b) H-plane radiation patterns for the boresight configuration. The maximum gain for the array in this configuration is 12.41 dBi.

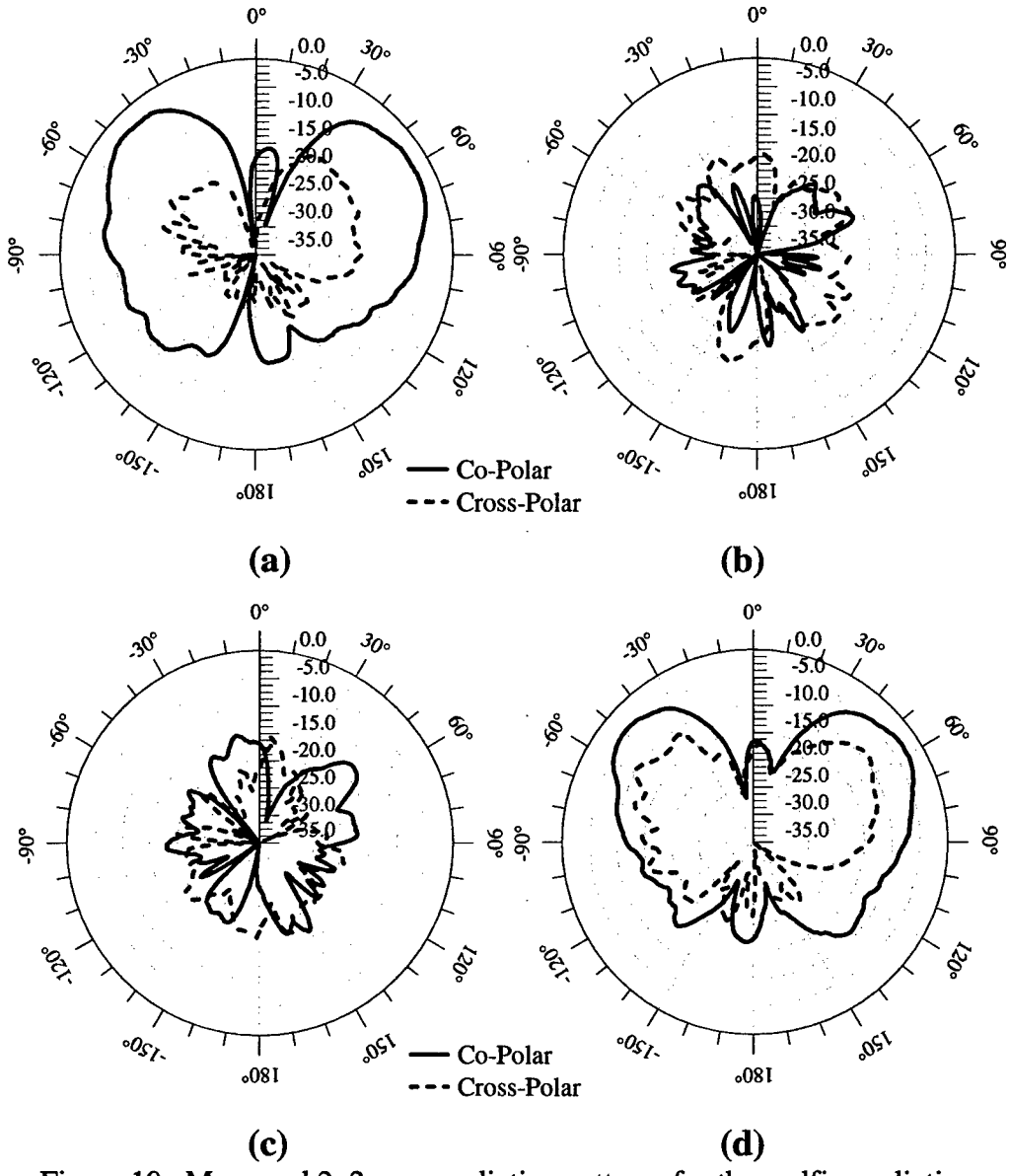

Figure 10. Measured 2x2 array radiation patterns for the endfire radiation configuration using two phasing routines; (a) and (b) are the E-plane and H-plane respectively for a 180° progressive phase shift in the E-plane (xz) and 0° in the H-plane (yx), (c) and (d) are the E-plane and H-plane respectively for a 180° progressive phase shift in the H-plane (yz) and 0° in the E-plane (xx). The maximum gain in (a) is 9.52 dBi and in (d) is 9.42 dBi, and is shown relative to the maximum radiation in the boresight configuration.